A model for the ultrasonic detection of surface-breaking cracks by the scanning laser-source technique

Irene Arias, Jan D. Achenbach

Irene Arias, Jan D. Achenbach, "A model for the ultrasonic detection of surface-breaking cracks by the scanning laser-source technique," Proc. SPIE 5393, Nondestructive Evaluation and Health Monitoring of Aerospace Materials and Composites III, (20 July 2004); doi: 10.1117/12.540109

SPIE.

Event: NDE for Health Monitoring and Diagnostics, 2004, San Diego, CA, United States

A model for the ultrasonic detection of surface-breaking cracks by the Scanning Laser-Source technique

Irene Arias[a] and Jan D. Achenbach[b]

[a]Graduate Aeronautical Laboratories, California Institute of Technology, 1200 E. California Blvd. MC: 205-45, Pasadena, CA 91125, USA;
[b]Center for Quality Engineering and Failure Prevention, Northwestern University, 2137 Sheridan Road, Evanston, IL 60208, USA

ABSTRACT

A model for the Scanning Laser Source (SLS) technique is presented. The SLS is a novel laser based inspection method for the ultrasonic detection of small surface-breaking cracks. The generated ultrasonic signal is monitored as a line-focused laser is scanned over the defect. Characteristic changes in the amplitude and the frequency content are observed. The modelling approach is based on the decomposition of the field generated by the laser in a cracked two-dimensional half-space, by virtue of linear superposition, into the incident and the scattered fields. The incident field is that generated by laser illumination of a defect-free half-space. A thermoelastic model has been used which takes account of the effect of thermal diffusion, as well as the finite width and duration of the laser source. The scattered field incorporates the interactions of the incident field with the surface-breaking crack. It has been analyzed numerically by a direct frequency domain boundary element method. A comparison with an experiment for a large defect shows that the model captures the observed phenomena.

Keywords: Laser ultrasonics, thermoelastic regime, line-source, surface-breaking crack, modelling, Scanning Laser Source technique

1. INTRODUCTION

Surface-breaking cracks in a structure can be ultrasonically detected using Lamb and Rayleigh waves. Conventional ultrasonic flaw detection methodologies require the generation of an ultrasonic wave packet that travels through a structure and interacts with existing flaws within the structure. Either reflected echoes or transmitted signals may be monitored in the pulse-echo or pitch-catch modes of operation.

In order to generate the wave packets for conventional pulse-echo and pitch-catch techniques, high-power pulsed lasers have emerged as versatile thermoelastic sources of ultrasound. The generation of ultrasound by laser irradiation provides a number of advantages over the conventional generation by piezoelectric transducers, namely high spatial resolution, non-contact generation and detection of ultrasonic waves, use of fiber optics, narrow-band and broad-band generation, absolute measurements, and ability to operate on curved and rough surfaces and at hard-to-access locations. On the receiving side, surface ultrasonic waves can be detected using piezoelectric (PZT) or EMAT transducers, or optical interferometers in a completely laser-based system. Ultrasound generated by laser irradiation contains a large component of surface wave motion, and is therefore particularly useful for the detection of surface-breaking cracks.

In both the pitch-catch and pulse-echo methods, the source is expected to generate a well established ultrasonic wave, which then interacts with existing flaws. The limitations on the size of the flaws that can be detected using these methods are determined by the ultrasonic reflectivity or transmittance of the flaw for the particular wavelength used, and by the sensitivity of the ultrasonic detector. As might be expected, small flaws give rise to weak reflections or small changes in the amplitude of transmitted signals, often too weak to be detected with existing laser detectors. The recently proposed Scanning Laser Source (SLS) technique,[1] provides an alternative inspection method which overcomes these size limitations.

Further author information: (Send correspondence to I.A.)
I.A.: E-mail: iarias@caltech.edu, Telephone: 1 626 395 4757
J.D.A.: E-mail: achenbach@northwestern.edu

Nondestructive Evaluation and Health Monitoring of Aerospace Materials and Composites III, edited by Peter J. Shull, Andrew L. Gyekenyesi, Proceedings of SPIE Vol. 5393 (SPIE, Bellingham, WA, 2004) · 0277-786X/04/$15 · doi: 10.1117/12.540109

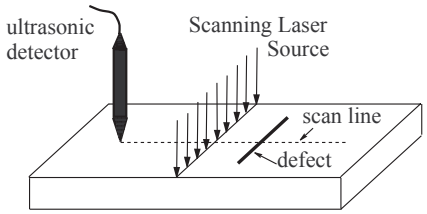

Figure 1. Configuration for the SLS technique.

The Scanning Laser Source (SLS) technique employs a line-focused high-power laser source which is swept across the test specimen and passes over surface-breaking anomalies.[2–4] The generated ultrasonic waves are detected with an ultrasonic detector located either at a fixed distance from the laser source or at a fixed position on the test specimen. Figure 1 sketches the inspection technique. The distinguishing feature of this method is that it monitors the changes in the laser generated signal as the illuminated region is swept over a defect, rather than the interactions of a well-established incident signal with the defect. The presence of a flaw modifies the generation conditions and produces reflections, leading to clear differences in the shape of the signal, its amplitude, and its frequency content, as compared to the signal generated on a defect-free surface. Thus, a distinct signature of the defect can be observed in the peak-to-peak amplitude and maximum frequency of the generated signal as the laser passes over the defect, as illustrated in the experimental observations and numerical simulations presented later in this paper. There is experimental evidence that this signature is noticeable even for cracks much smaller than the detection threshold for conventional methods and for arbitrary orientation of the crack with respect to the direction of scanning.[2]

In this paper, a model for the SLS technique is presented and compared against experiments. The objective is to identify the relevant physical mechanisms responsible for the observed behavior, and possibly optimize the inspection technique. Section 2 describes the modelling approach. Section 3 presents comparisons with experiments. We sum up and close in Section 4.

2. THEORETICAL APPROACH

The development of a model for the SLS technique starts with the solution of the problem of laser generation of ultrasound in the presence of a discontinuity. We have considered the two dimensional problem of an infinitely long thermoelastic laser line source impinging on an isotropic, homogeneous, linearly elastic half-space with an infinitely long, mathematically sharp crack both perpendicular to the surface of the half-space and parallel to the line source. By virtue of linear superposition, the complete problem of obtaining the total field generated by a laser source impinging on a half-space in the presence of a surface breaking crack can be decomposed into two subproblems (see Fig. 2). The first one entails obtaining the so-called incident field which is generated by the laser source impinging on an uncracked half-space. The second involves the determination of the so-called scattered field, which is generated in the cracked half-plane by the application of tractions on the crack faces which are equal in magnitude and opposite in sign to the corresponding tractions due to the incident field in the uncracked half-plane.

2.1. The Incident Field

In previous work,[5] we developed a theoretical model for the field generated by laser illumination in the thermoelastic regime which takes account of the finite width of the source, the temporal shape of the pulse and the subsurface sources arising from thermal diffusion and optical penetration. The effects of thermal diffusion and optical penetration, negligible in the far-field, are quite important in the vicinity of the generation source. Note that the key processes leading to the signature of the defect monitored by the SLS technique result from the interaction of the laser-generated near field with the defect. Thus, it is essential to capture the near-field effects for our purposes. In metals, the subsurface sources arise mainly from thermal diffusion, since the optical absorption depth is very small compared to the thermal diffusion length. In ceramics and other non-metallic

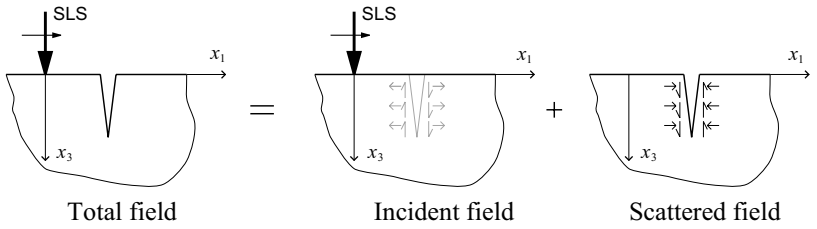

Figure 2. Decomposition of the total field into incident and scattered fields.

materials, roles reverse and optical penetration becomes the main mechanism of energy deposition below the surface. In this paper, we focus on metals and thus neglect the effect of optical penetration.

The thermoelastic problem is formulated in the context of the generalized theory of thermoelasticity which assumes a hyperbolic description of heat conduction. The governing equations of the thermal and the elastic problems are in principle doubly coupled. However, in the thermoelastic regime, the heat produced by mechanical deformation can be neglected. With this so-called thermal stress approximation, the equations are coupled only one-way through the thermal stress term. The governing equations for an isotropic solid are:

$$\nabla^2 T - \frac{1}{\kappa}\,\dot{T} - \frac{1}{c^2}\,\ddot{T} = -\frac{q}{k}, \tag{1}$$

$$\mu\nabla^2\mathbf{u} + (\lambda+\mu)\nabla(\nabla\cdot\mathbf{u}) = \rho\ddot{\mathbf{u}} + \beta\nabla T, \tag{2}$$

where T is the absolute temperature, $\mathbf{u}$ is the displacement vector field, κ is the thermal diffusivity, c is the heat propagation speed which is taken to be equal to the longitudinal wave speed (see Ref. 5 for details), k is the thermal conductivity, β is the thermoacoustic coupling constant: $\beta = (3\lambda+2\mu)\alpha_T$, α_T is the coefficient of linear thermal expansion and q is the heat source due to laser line-source illumination. A suitable expression for the surface heat deposition q in the solid along an infinitely long line is

$$q = E(1-R_i)\,\frac{2}{R_G\sqrt{2\pi}}\,e^{-2x_1^2/R_G^2}\,\frac{8t^3}{\upsilon^4}\,e^{-2t^2/\upsilon^2}, \tag{3}$$

where E is the energy of the laser pulse per unit length, R_i is the surface reflectivity, R_G is the Gaussian beam radius, υ is the laser pulse risetime (full width at half maximum). The coordinate axis x_1 is directed along the surface perpendicularly to the line-source, and x_3 normal to the surface pointing inwards.

Equation (3) represents a strip of illumination since it is defined by a Gaussian in x_1. The Gaussian does not vanish completely with distance, but its value becomes negligible outside a strip. The source is spread out in time according to the function proposed by Schleichert and co-workers.[6] For both the temporal and the spatial profile, the functional dependence has been constructed so that in the limit $\upsilon \to 0$ and $R_G \to 0$, an equivalent concentrated line-source is obtained.

Equations (1–3) with the appropriate boundary and initial conditions are solved for the case of line illumination of an isotropic, homogeneous, linearly elastic half-space by a semi-analytical procedure using standard Fourier-Laplace transform techniques.[5]

Figure 3 illustrates a stress-field solution of the above problem. The laser generation of ultrasound can be understood as follows. Initially, a large amount of heat is very rapidly deposited in a thin strip of material. Heat diffusion time-scales are much larger than the duration of the heat deposition, and consequently, a localized portion of the material undergoes a rapid expansion, constrained by the surrounding unheated material. This in turn generates ultrasonic elastic waves. It is clear from the snapshots, that while elastic wave propagation dominates the far-field solution, near the source thermal stresses hide the wave patterns. A more detailed analysis of these solutions reveals that simplified approaches based on equivalent stress dipoles are inaccurate in the near field.[5]

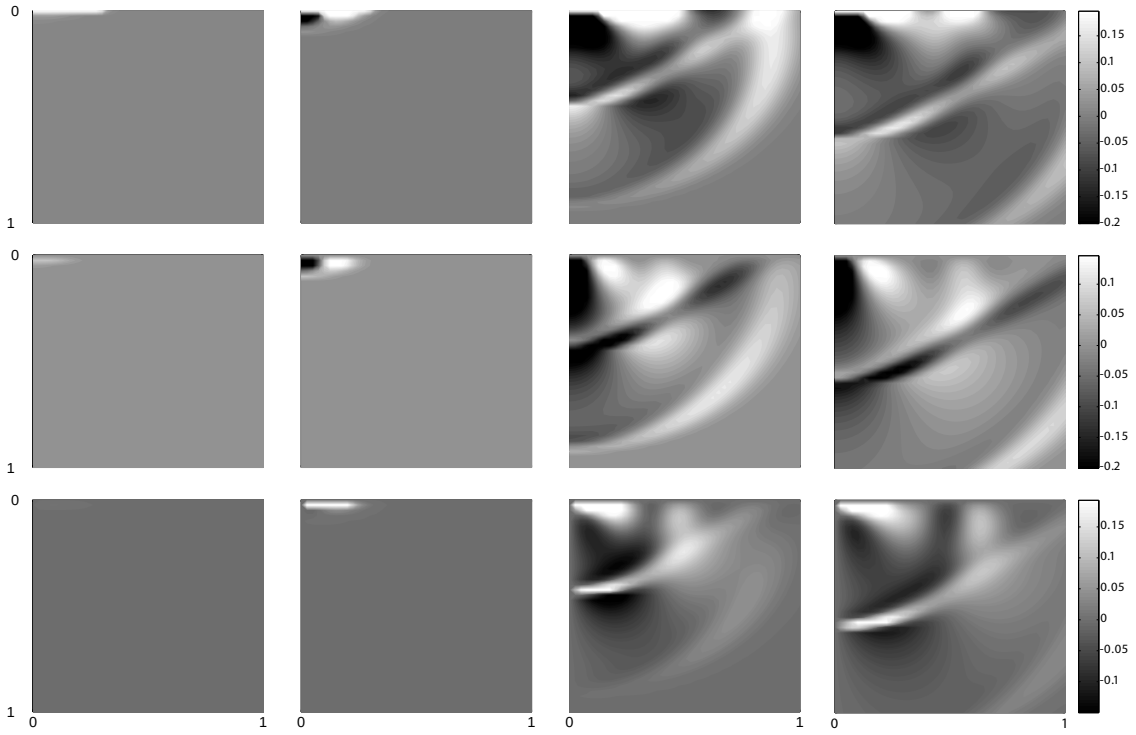

Figure 3. Snapshots of the stress components σ_{11} (top), σ_{33} (middle) and σ_{31} (bottom) due to the laser line-source at times 0.01 (left), 0.02 (center-left), 0.15 (center-right) and 0.2 μs (right), computed for $R_G = 0.45$ mm and $\upsilon = 10$ ns. The region shown corresponds to 1 mm in depth per 1 mm to the right of the epicentral axis. Positive normal stresses indicate compression.

2.2. The Scattered Field

The interactions of a surface-breaking crack with the field generated by the laser in a half-space are analyzed next. By decomposing the scattered field into symmetric and anti-symmetric fields with respect to the plane of the crack, two initial boundary value problems for the quarter-space are obtained (see Fig. 4). The symmetric problem is defined by normal tractions acting on the plane of the crack which are equal and opposite to the ones generated by the incident field, whereas the anti-symmetric problem is defined by the corresponding shear tractions. Therefore, the boundary conditions at $x_1 = 0$ for each problem are:

$$\sigma_{13}^{\mathrm{sc}} = 0, \quad 0 \le x_3 < \infty, \qquad \sigma_{11}^{\mathrm{sc}} = -\sigma_{11}^{\mathrm{in}}, \quad 0 \le x_3 < a, \qquad u_1^{\mathrm{sc}} = 0, \quad a \le x_3 < \infty \tag{4}$$

for the symmetric problem and

$$\sigma_{13}^{\mathrm{sc}} = -\sigma_{13}^{\mathrm{in}}, \quad 0 \le x_3 < a, \qquad \sigma_{11}^{\mathrm{sc}} = 0, \quad 0 \le x_3 < \infty, \qquad u_3^{\mathrm{sc}} = 0, \quad a \le x_3 < \infty \tag{5}$$

for the anti-symmetric problem, where the superscripts "sc" and "in" stand for the scattered, and the incident fields respectively and a is the length of the crack. For both the symmetric and the anti-symmetric problem, the surface of the quarter-space is free of tractions. In addition, it is required that the scattered field represents outgoing waves. The governing equation for a homogeneous, isotropic, linearly elastic solid is Eq. 2, which in the isothermal case reduces to:

$$\mu \nabla^2 \mathbf{u}^{\mathrm{sc}}(\mathbf{x}, t) + (\lambda + \mu) \nabla (\nabla \cdot \mathbf{u}^{\mathrm{sc}})(\mathbf{x}, t) = \rho \ddot{\mathbf{u}}^{\mathrm{sc}}(\mathbf{x}, t), \tag{6}$$

where $\mathbf{x} \in (-\infty, 0] \times [0, \infty)$ is the position vector and $t > 0$ represents time.

Each of these problems is solved numerically with a two-dimensional direct frequency domain quadratic boundary element method.[7] The symmetric and anti-symmetric problems are formulated in the frequency

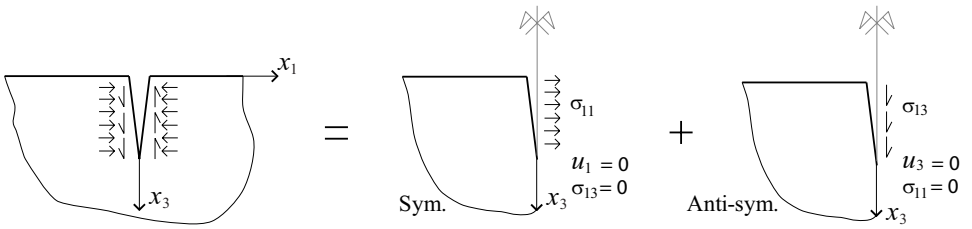

Figure 4. Decomposition into the symmetric and the anti-symmetric problems in a quarter-space.

domain by the application of the Fourier transform to the equation and the boundary conditions, assuming a quiescent past. The resulting transformed equation of motion is:

$$\mu\nabla^2\bar{\mathbf{u}}^{\mathrm{sc}}(\mathbf{x},\omega) + (\lambda+\mu)\nabla(\nabla\cdot\bar{\mathbf{u}}^{\mathrm{sc}})(\mathbf{x},\omega) + \rho\omega^2\bar{\mathbf{u}}^{\mathrm{sc}}(\mathbf{x},\omega) = 0, \tag{7}$$

where ω stands for the angular frequency and the transformed displacement field is denoted with a bar. The corresponding boundary integral equations for a point $\boldsymbol{\xi}$ located on the boundary of the domain, Γ, are derived in the usual manner[8] as:

$$c_{\alpha\beta}(\boldsymbol{\xi})\,\bar{u}^{\mathrm{sc}}_{\beta}(\boldsymbol{\xi},\omega) = \int_{\Gamma}\left[\bar{u}^{*}_{\alpha\beta}(\boldsymbol{\xi},\mathbf{x},\omega)\,\bar{t}^{\mathrm{sc}}_{\beta}(\mathbf{x},\omega) - \bar{t}^{*}_{\alpha\beta}(\boldsymbol{\xi},\mathbf{x},\omega)\,\bar{u}^{\mathrm{sc}}_{\beta}(\mathbf{x},\omega)\right]d\Gamma(\mathbf{x}),$$
$$\alpha,\beta = 1,2, \tag{8}$$

where $\bar{u}^{*}_{\alpha\beta}$ and $\bar{t}^{*}_{\alpha\beta}$ are the full-space frequency domain elastodynamic fundamental solution displacement and traction tensors respectively. Note that $\bar{u}^{*}_{\alpha\beta}(\boldsymbol{\xi},\mathbf{x},\omega)$ and $\bar{t}^{*}_{\alpha\beta}(\boldsymbol{\xi},\mathbf{x},\omega)$ represent the "β" component of the displacement and the traction on the boundary, respectively, at the point $\mathbf{x}$ due to a unit time-harmonic load of angular frequency ω applied at the point $\boldsymbol{\xi}$ in the direction "α". Also, $\bar{u}^{\mathrm{sc}}_{\beta}$, $\bar{t}^{\mathrm{sc}}_{\beta}$ are frequency domain displacements and tractions on the boundary, and $c_{\alpha\beta}$ is called the jump coefficient given by:

$$c_{\alpha\beta}(\boldsymbol{\xi}) = \begin{cases} \frac{1}{2}\delta_{\alpha\beta}, & \text{if } \Gamma \text{ is smooth at } \boldsymbol{\xi}, \\ c_{\alpha\beta}, & \text{if } \Gamma \text{ has a corner at } \boldsymbol{\xi}, \end{cases} \tag{9}$$

where $\delta_{\alpha\beta}$ represents the Kronecker delta. The jump coefficient for corner points can be derived by an indirect approach as described in Ref. 8. The integrals in Eq. (8) are interpreted in the sense of the Cauchy Principal Value.

The boundary integral equations are solved numerically for the symmetric and anti-symmetric transformed displacements and tractions on the boundary. The boundary of the domain is discretized using quadratic boundary elements and a quadratic interpolation of the transformed displacements and traction fields is introduced. A singular traction quarter-point boundary element has been used to reproduce the singular behavior of the stresses at the crack tip.[9] After solving the transformed problems, the transient solution is obtained by numerical inversion of the Fourier transform with a fast Fourier transform (FFT) algorithm.

Note that the above presented approach entails the solution of two initial boundary value problems on the quarter-space, instead of just one on the half-space. However, it avoids the well-known degeneracy of the conventional BEM for the flat cracks, which is essentially associated with the ill-posed nature of problems with two coplanar faces.[10]

It has been shown that the sharpness of the laser line-source generated signal increases as the line becomes narrower or the laser pulse shorter.[5] For instance, in the limit of the shear dipole, the generated Rayleigh surface wave is a monopolar pulse propagating along the surface of the half-space which reproduces the shape of the laser pulse. The high-frequency content of the incident field for narrow lines and short pulses imposes stringent conditions on the number of frequencies to be computed for an accurate sampling in a given time window. The requirement of describing a wavelength with about 10 nodes results in a quite small element size. On the other hand, in experiments the receiver is located at sufficient distance from the crack to allow for the scanning of the

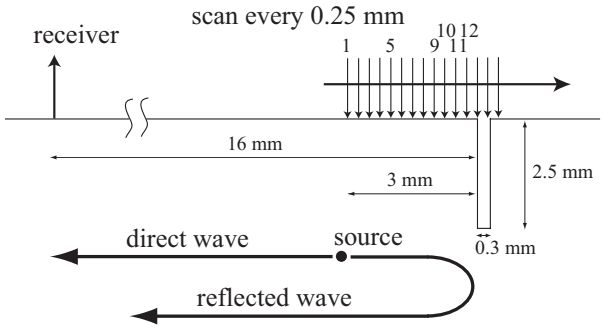

Figure 5. Experimental setup for the SLS inspection of a notched specimen.

specimen surface, and thus the region of interest, where accurate solutions are needed, can be relatively large, leading to a high number of elements. These facts lead to large computational meshes and, thus, high memory requirements and computational times. In efforts to reduce the computational time, the natural parallelism of the frequency domain approach has been exploited in the computer implementation.

The infinite surface of the quarter-space has to be truncated for numerical calculation purposes. The simple truncation introduces spurious reflections from the ends of the computational boundary that distort the numerical solution in the region close to the truncation point. Note that in a two-dimensional geometry, undamped Rayleigh waves do not exhibit geometrical attenuation, and will always produce reflections in a simply truncated mesh. This issue is typically addressed by extending the computational mesh far beyond the region of interest and adding a small amount of damping. In Ref. 11 a correction for the truncation of the infinite boundary has been formulated which allows the undamped Rayleigh waves to escape the computational domain without producing spurious reflections from its end nodes.

3. COMPARISON WITH EXPERIMENT

Sohn and Krishnaswamy[12] have carried out experiments on an aluminum specimen in the presence of a notch of 2.5 mm in depth and 0.3 mm in width. A Q-switched line-focused laser was used at 10 mJ energy deposition. The width of the illumination strip was estimated to be around 200 μm width by burn marks on photosensitive paper. The duration of the pulse was 70 ns. The laser source scanned the specimen from a distance of 3.0 mm from the left face of the notch to a distance of 0.5 mm past the left face of the notch. A laser detector was used to record surface normal displacements at a distance of 16 mm from the left face of the crack in each scanning step (see Fig. 5). Both the signals recorded at the receiver and the resulting peak-to-peak amplitude evolution with the position of the laser source were provided.

A numerical example inspired in this experiment is presented next. The notch has been replaced by a surface-breaking crack of the same depth in the plane of the left face of the notch. It has been verified, that this approximation does not have a significant effect on the response of the system at the receiver for a notch of this depth relative to the wavelengths of the generated Rayleigh wave. The material properties used in the simulation are: $c_L = 5.9$ mm/μs, $c_T = 3.1$ mm/μs, $\alpha_T = 2.2 \cdot 10^{-5}$ 1/K, $\kappa = 1.0 \cdot 10^{-4}$ mm^2/μs, $k = 160$ W/mK, $R_i = 91\%$. There are uncertainties concerning the exact spatial and temporal distribution of the energy deposition. Thus, the parameters of the laser source model have been selected to approximately reproduce the direct signal from the laser source.

Figs. 6 and 7 show the experimental (left column), and the numerically predicted (right column) signals at the receiver when the laser is located at six different positions relative to the left face of the notch. The receiver is far enough so that most of the recorded waveforms correspond to Rayleigh waves. In the first plots, the monopolar direct signal and the reflection can be clearly distinguished. As the laser approaches the notch, these signals start to interfere with each other. An apparent increase in peak to peak amplitude and a sharp outward surface displacement can be observed when the laser is close to the crack. Experiment and simulation show good

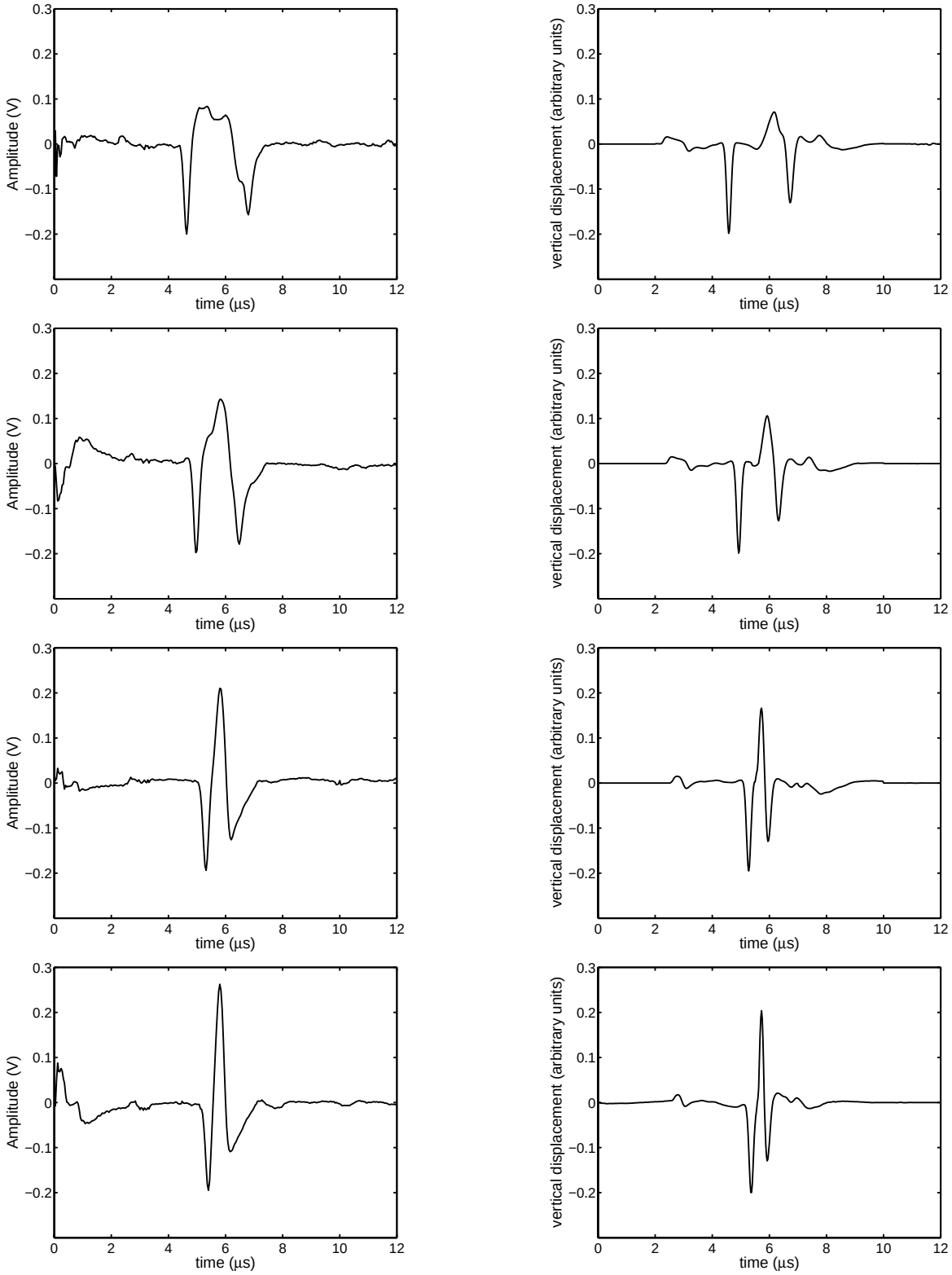

Figure 6. Experimental (left column) and simulated (right column) signals at the receiver when the laser is located at distances of 3, 2, 1 and 0.75 mm from the left face of the notch.

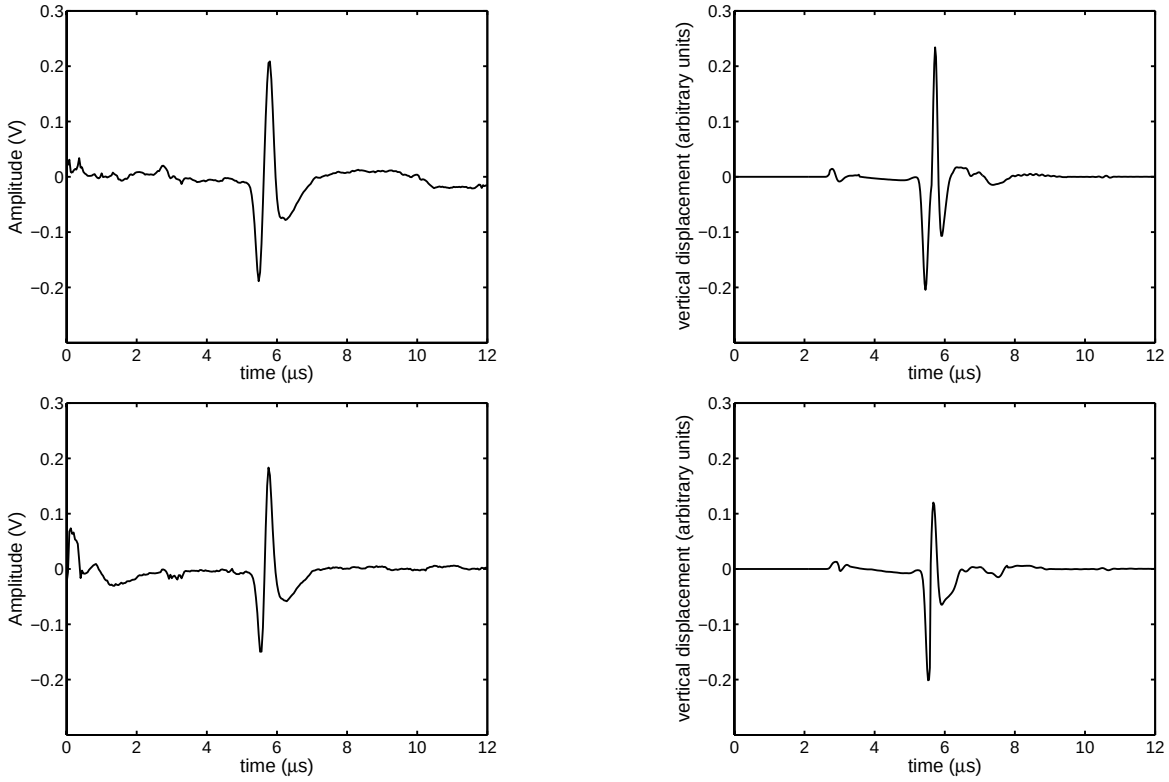

Figure 7. Experimental (left column) and simulated (right column) signals at the receiver when the laser is located at distances of 0.5 and 0.25 mm from the left face of the notch.

qualitative agreement. Better quantitative agreement would follow from further adjustment of the parameters of the model.

Fig. 8 shows the experimental and numerical evolution of the peak to peak amplitude. The characteristic signature of the discontinuity is well predicted by the model. Due to the large depth of the crack, a very small signal is predicted when the laser impinges of the right side of the notch. This signal cannot be distinguished from experimental records.

4. CONCLUSIONS

A model for the Scanning Laser Source (SLS) technique for the ultrasonic detection of surface-breaking cracks has been presented. The generation of ultrasound by a line-focused laser source on a two-dimensional homogeneous, isotropic, linearly elastic half-space in the presence of a surface-breaking crack has been analyzed. The modelling approach is based on a decomposition of the generated field in the presence of the defect into the incident and the scattered fields. The incident field is that generated by the laser on a defect-free half-space. A thermoelastic model has been used which takes account of the effects of thermal diffusion from the source, as well as the finite width and duration of the laser source. The scattered field incorporates the interactions of the incident field with the discontinuity. It has been analyzed numerically by the boundary element method. A special treatment of the infinite boundary has been used which eliminates spurious reflections from the ends of the computational boundary. The SLS simulations are obtained by superposition of these two fields.

It is shown that the experimentally observed features characterizing the presence and size of surface-breaking cracks are well reproduced by the model. A comparison of experimental and simulated signals at the receiver for the case of a large notch shows good qualitative agreement. Further adjustment of the parameters of the model is needed for a better quantitative agreement.

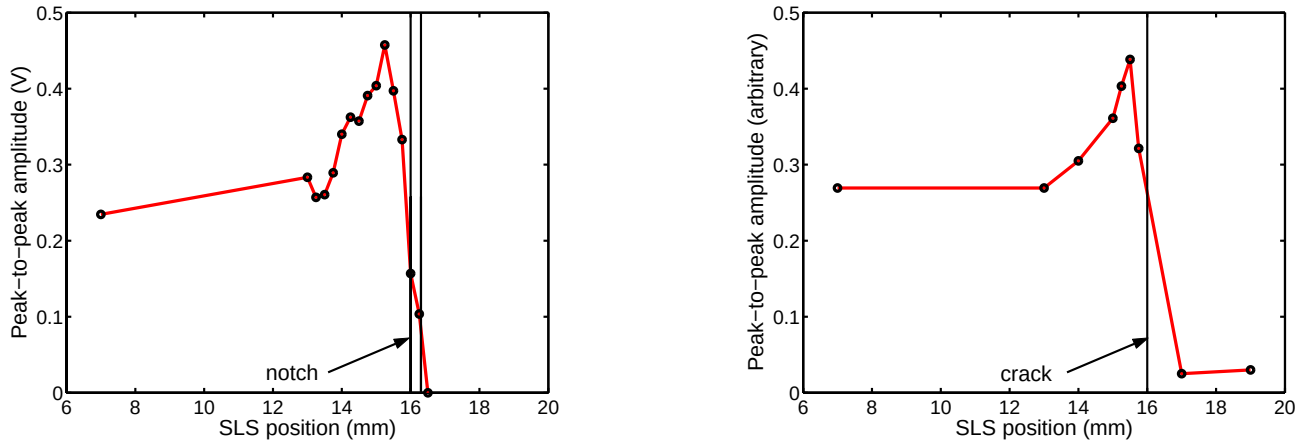

Figure 8. Experimental (left) and simulated (right) peak-to-peak amplitude vs. position of the source relative to the crack (SLS position).

ACKNOWLEDGMENTS

This work was carried out in the course of research funded by the Federal Aviation Administration under Contract #DFTA 03-98-D-0008 through the Air Transportation Center of Excellence in Airworthiness Assurance.

REFERENCES

1. A. Kromine, P. Fomitchov, S. Krishnaswamy, and J. Achenbach, "Laser ultrasonic detection of surface breaking discontinuities: scanning laser source technique," *Materials Evaluation* **58**(2), pp. 173–177, 2000.
2. A. Kromine, P. Fomitchov, S. Krishnaswamy, and J. Achenbach, "Scanning laser source technique for detection of surface-breaking and sub-surface cracks," in *Review of Progress in Quantitative Nondestructive Evaluation*, D. Thompson and D. Chimenti, eds., **19**, pp. 335–342, AIP Press, New York, 2000.
3. A. Kromine, P. Fomitchov, S. Krishnaswamy, and J. Achenbach, "Detection of subsurface defects using laser based technique," in *Review of Progress in Quantitative Nondestructive Evaluation*, D. Thompson and D. Chimenti, eds., **20**, pp. 1612–1617, AIP Press, New York, 2001.
4. P. Fomitchov, A. Kromine, Y. Sohn, S. Krishnaswamy, and J. Achenbach, "Ultrasonic imaging of small surface-breaking defects using scanning laser source technique," in *Review of Progress in Quantitative Nondestructive Evaluation*, D. Thompson and D. Chimenti, eds., **21**, pp. 356–362, AIP Press, New York, 2002.
5. I. Arias and J. Achenbach, "Thermoelastic generation of ultrasound by line-focused laser irradiation," *International Journal of Solids and Structures* **40**, pp. 6917–6935, 2003.
6. U. Schleichert, K. Langenberg, W. Arnold, and S. Fassbender, "A quantitative theory of laser-generated ultrasound," in *Review of Progress in Quantitative Nondestructive Evaluation*, D. Thompson and D. Chimenti, eds., **8A**, pp. 489–496, AIP Press, New York, 1989.
7. Y. Niwa, S. Hirose, and M. Kithara, "Application of the boundary integral equation (bie) method to transient response analysis of inclusions in a half-space," *Wave Motion* **8**, pp. 77–91, 1986.
8. J. Domínguez, *Boundary elements in dynamics*, Computational mechanics publications, Elsevier applied science, 1993.
9. G. Blandford, A. Ingraffea, and J. Liggett, "Two-dimensional stress intensity factor computations using the boundary element method," *International Journal for Numerical Methods in Engineering* **17**, pp. 387–404, 1981.
10. T. Cruse, Fracture Mechanics. In *Boundary element methods in mechanics*, pp. 333–365. North-Holland, Amsterdam, 1987. D.E. Beskos (ed.).
11. I. Arias and J. Achenbach, "Rayleigh wave correction for the BEM analysis of two-dimensional elastodynamic problems in a half-space," *International Journal for Numerical Methods in Engineering* , 2004. in press.
12. Y. Sohn and S. Krishnaswamy *Private communication* , 2003.